Materials Science and Engineering C 58 (2016) 204–212

Contents lists available at ScienceDirect

Materials Science and Engineering C

journal homepage: www.elsevier.com/locate/msec

Functionalization of polycaprolactone/hydroxyapatite scaffolds with *Usnea lethariiformis* extract by using supercritical CO_2

M.A. Fanovich [a,*], J. Ivanovic [b], I. Zizovic [b], D. Misic [c], P. Jaeger [d]

[a] INTEMA (Univ. Nacional de Mar del Plata — CONICET), Av. J.B.Justo 4302, 7600 Mar del Plata, Argentina
[b] University of Belgrade, Faculty of Technology and Metallurgy, Karnegijeva 4, 11000 Belgrade, Serbia
[c] University of Belgrade, Faculty of Veterinary Medicine, Bulevar Oslobodjenja 18, 11000 Belgrade, Serbia
[d] Inst. Thermal Process Engineering, Hamburg University of Technology, Eißendorfer Str. 38, 21073 Hamburg, Germany

ARTICLE INFO

Article history:
Received 27 January 2015
Received in revised form 3 April 2015
Accepted 14 August 2015
Available online 16 August 2015

ABSTRACT

Investigation of an integrated supercritical fluid extraction and supercritical solvent impregnation process for fabrication of microporous polycaprolactone–hydroxyapatite (PCL–HA) scaffolds with antibacterial activity is presented. The HA content and particle size as well as the operating conditions of the integrated process is optimized regarding the amount of impregnated antibacterial agent (*Usnea lethariiformis* extract) in the PCL–HA matrix, scaffold morphology and antibacterial activity against methicillin resistant *Staphylococcus aureus* (MRSA) strains. High pressure differential scanning calorimetry (HP-DSC) assay reveals that an increasing amount of HA results in decreasing melting temperature as well as crystallinity at an operating pressure of 17 MPa. The PCL–HA composites with micrometric sizes of the HA particles are convenient for being processed by the integrated process due to the simple preparation, a good interaction between the PCL matrix and filler and the advantageous impact on sorption. The scaffold obtained from PCL–HA with 20% of the HA shows the highest impregnation yield at 17 MPa and 35 °C (5.9%) and subsequently also the best bactericidal effect on the tested MRSA strains at an initial bacterial inoculum of 2×10^{-4} CFU/mL.

1. Introduction

Over the past several decades, an increase of the worldwide incidence of bone disorders has led to a great interest in the development of alternative materials for grafts due to their limitless supply and their security for the no transmission of diseases [1]. Polymer and calcium phosphate ceramic composites have been especially attractive for the scaffold fabrication due to their composition combining favorable properties of the both phases [2]. Hydroxyapatite (HA), $Ca_{10}(PO_4)_6(OH)_2$, is the most frequently used calcium phosphate in the biomedical composites due to its excellent properties such as osteoconductivity and bioactivity [3]. These characteristics promote the use of HA powders in different composite materials with the objective of increasing the degree of bioactivity and thus enhancing the performance of the developed new materials [4–9]. On the other hand, polycaprolactone (PCL) is a biodegradable and biocompatible semi-crystalline polyester that has been widely proposed for fabrication of scaffolds in the bone tissue engineering (bTE) [10]. Due to their individual properties, the combination of HA and PCL holds a great potential for fabrication of bioactive load-bearing scaffolds [4,11–13].

Porous PCL–HA scaffolds are commonly fabricated by the solvent casting technique [5,14] from a polymer melt [11,15], which involves usage of porogens (salt particles, paraffin microspheres or emulsion particles), molding and solvent removal by evaporation or lyophilisation. The main limitation of the conventional techniques for scaffold fabrication is related with the difficulty to obtain the desired macro, micro- and nanostructure simultaneously [16]. Also, the residual organic solvents should be considered. Various techniques using supercritical carbon dioxide ($scCO_2$) can be employed to exclude or eliminate organic solvents and enable control of scaffold morphologies thanks to tunable properties of dense gases and modulability of mass transfer in corresponding systems. Among these techniques are supercritical foaming, supercritical assisted phase separation, processes based on solvent elimination by $scCO_2$-gel drying, electrospinning and emulsion templating in $scCO_2$ [16–19].

Further, it is possible to introduce bioactive molecules during polymer processing with the help of $scCO_2$, as a way of functionalizing these. In order to obtain antibacterial properties, diverse studies focused on incorporation of antibacterial agents into scaffolds mainly by conventional methods [20,21] and only recently high interest is gained in bioactive plant extracts that are processed with $scCO_2$ [22–26]. This aspect opens a range of possibilities for developing new composite materials with specific properties. When functionalizing composite materials by using $scCO_2$ it is very important to understand and predict the

* Corresponding author.
E-mail addresses: mafanovi@fi.mdp.edu.ar (M.A. Fanovich), zizovic@tmf.bg.ac.rs (I. Zizovic).

http://dx.doi.org/10.1016/j.msec.2015.08.024
0928-4931/

transport of CO_2 in this new environment, basically because the CO_2 acts as a carrier for active substances. Markočič et al. [27] determined the solubility and diffusivity of CO_2 in heterogeneous systems (PLLA-HA and PLGAHA composites) that showed high values of both parameters influenced by the CO_2 pressure and the content of the ceramic filler. The presence of the filler particles changes the overall structure of the matrix which on its turn takes influence on the sorption procedure by modifying the path of diffusing molecules. In case of a good contact between polymer and filler, the solubility of gas in the polymer matrix is decreased since the filler particles act as obstacles reducing free volume (the polymer "wets" the filler particles and the solid particles occupy the free volume otherwise available to the absorbed gas). In case the filler particles are not perfectly integrated, i.e., not completely wetted or contacted by the polymer, it may lead to appearance of voids in the structure providing an enlarged interface available to gas sorption, which increases solubility and diffusivity [28]. In this sense, the morphology and size of filler particles are relevant features for determining the interaction between the filler and the matrix, and consequently, the mass transport of $scCO_2$ differs from the pure polymer. By controlling the volume fractions and the distribution of the inorganic filler the behavior of a composite biomaterial can be varied and tailored.

Actually, the development of porous structures by using supercritical carbon dioxide is accepted as an interesting processing option for biomaterials and has been successfully implemented to produce homogeneous foams with controlled pore structures, especially for polymeric materials [18,29–32]. The concentration of CO_2 dissolved in the material is one of the main factors that influence the characteristics of the obtained foam. Also, by simple variation of the processing parameters (pressure, temperature, depressurization rate) it is possible to control the size and distribution of the pores in the obtained material [32].

The aim of this work was to develop PCL–HA composite scaffolds functionalized with a natural extract giving antibacterial properties to the new biomaterial. First, the behavior under CO_2 pressure of PCL–HA composites with different particle sizes of HA was analyzed in terms of melting temperature and crystallinity by using high pressure differential scanning calorimeter (HP-DSC). Thereafter, a process for functionalizing PCL–HA composites containing 10 and 20 wt.% HA was applied. The antibacterial substance for impregnation (*Usnea lethariiformis* extract) was extracted from a Patagonian lichen. The used methodology is described elsewhere [30] as an integrated process where three steps are integrated in one procedure (extraction–impregnation–formulation) and applied on PCL–HA composites. The influence of processing conditions was analyzed with respect to the impregnation weight percent, morphology and antibacterial activity of the PCL–HA scaffolds against methicillin resistant *Staphylococcus aureus* (MRSA) strains.

2. Materials and methods

2.1. Materials

Granules of PCL (Mn = 70,000–90,000) were purchased from Sigma Aldrich (Germany) CAS 24980-41-4. Patagonian lichen *U. lethariiformis* (voucher specimens No 16644, Herbarium of Institute of Botany and Botanical Garden Jevremovac, Faculty of Biology, University of Belgrade) collected in Ushuaia, Tierra del Fuego (Argentinian Republic) in 2011 (GPS −54.544221–67.202307) was used to extract antibacterial substances using $scCO_2$ for scaffolds impregnation. Commercial carbon dioxide (99% purity) supplied by Gamasol (Argentine) was used for all supercritical processes.

Hydroxyapatite powders were obtained by a precipitation method as described elsewhere [33]. The starting materials were analytical grade: $CaCO_3$ (99%, PA Cicarelli) as the Ca source and H_3PO_4 (85%, Merck) as the P source. The $CaCO_3$ was thermally treated in an oven (Indef, model 332 p-full) at 1200 °C for 2 h to obtain CaO. The solid CaO was first dispersed in ammonium hydroxide (pH = 12) and subjected to conventional mechanical stirring. Subsequently, H_3PO_4 0.5 mol/L was slowly added dropwise into the same beaker at 2 mL/min until reaching a molar ratio of Ca/P = 1.67 with conventional mechanical stirring (M) or ultrasonic irradiation treatment (S). After this step, the reaction mixture was kept at an aging step during 48 h. Finally, the precipitate was centrifuged and freeze-dried. Two types of filler particles were obtained: HA(M) (mean particle size of 10 μm; specific surface area of 15 m^2/g) and HA(S) (mean particle size of 5 μm; specific surface area of 33 m^2/g). Nano-HA powder, HA(N) (mean particle size of <1 μm; specific surface area of 70 m^2/g) was obtained by the López Macipe method [34].

2.2. Preparation of PCL–HA composites

The obtained HA powders were added to a solution of PCL/acetone (1:10) and dispersed with the Ultra Turrax T25 (IKA, Germany) at 20,000 rpm during 10 min. The nominal content of HA added to PCL/acetone solution was 10% or 20% with respect to the PCL weight. The solvent was evaporated at room temperature under a fume hood. The obtained composite films were pelletized and used for analysis in a high pressure differential scanning calorimetry (HP-DSC) and for $scCO_2$ processing, both described below.

2.3. High pressure differential scanning calorimetry on PCL and PCL–HA composites

The low temperature Tian-Calvet differential scanning calorimeter BT2.15 (Setaram, France) was used for these measurements. The operating range is −196 °C to 200 °C. The BT 2.15 is equipped with an integrated liquid nitrogen cooling loop for operation at sub-ambient temperatures. The calorimeter contains two heat flux meters consisting of a series of thermocouples surrounding a cylindrical cavity. These devices are arranged symmetrically around a reference cell and a sample cell in an aluminum block located in the cavity. The signal delivered by the power difference of the two flux meters is proportional to the heat effects occurring in the cells. The DSC is coupled with a gas control panel that can withstand maximum pressures of 20 MPa.

Standard stainless steel vessels (V = 12 cm^3, P_{max} = 0.5 MPa, T_{max} = 220 °C) and intermediate bottom stainless steel vessels (V = 8.5 cm^3, P_{max} = 0.5 MPa, T_{max} = 220 °C) were used for the measurements at atmospheric conditions. High pressure vessels made of Inconel 625 (V = 3.6 cm^3, P_{max} = 60 MPa, T_{max} = 500 °C) were used for measurements at higher pressures in the range of 5–17 MPa. The sample was heated at a rate of 0.10 °C/min over a temperature range from room temperature (22–25 °C) °C to 85 °C. An empty, hermetically sealed stainless steel pan was used as a reference. Melting point and enthalpies of indium were used for temperature and heat capacity calibration. The crystallinity of PCL phase in the composite (X_c) was determined using a heat of fusion value of the PCL–HA composite calculated from a DSC curve using the Calisto Data Acquisition software (Version 1.071) and heat of fusion of 100% crystalline PCL (ΔH_m^o = 135.31 J/g [35]) according to the Eq. (1).

$$X_c(\%) = \frac{\Delta H_m}{\Delta H_m^o} \times 100. \quad (1)$$

2.4. Integrated extraction–impregnation process with $scCO_2$

The process for impregnation of composites with antibacterial lichen extracts after supercritical fluid extraction thereof is shown in Fig. 1. This laboratory scale unit (HPEA 500, Eurotechnica, Germany) has been designed for an integrated extraction–impregnation process and was extended by closing the solvent (supercritical CO_2) cycle in a way that the included extractor (E, 500 mL) and an the adsorption column (A, 100 mL) can be operated at different temperatures and pressures independently from each other. The extractor vessel is filled with the raw

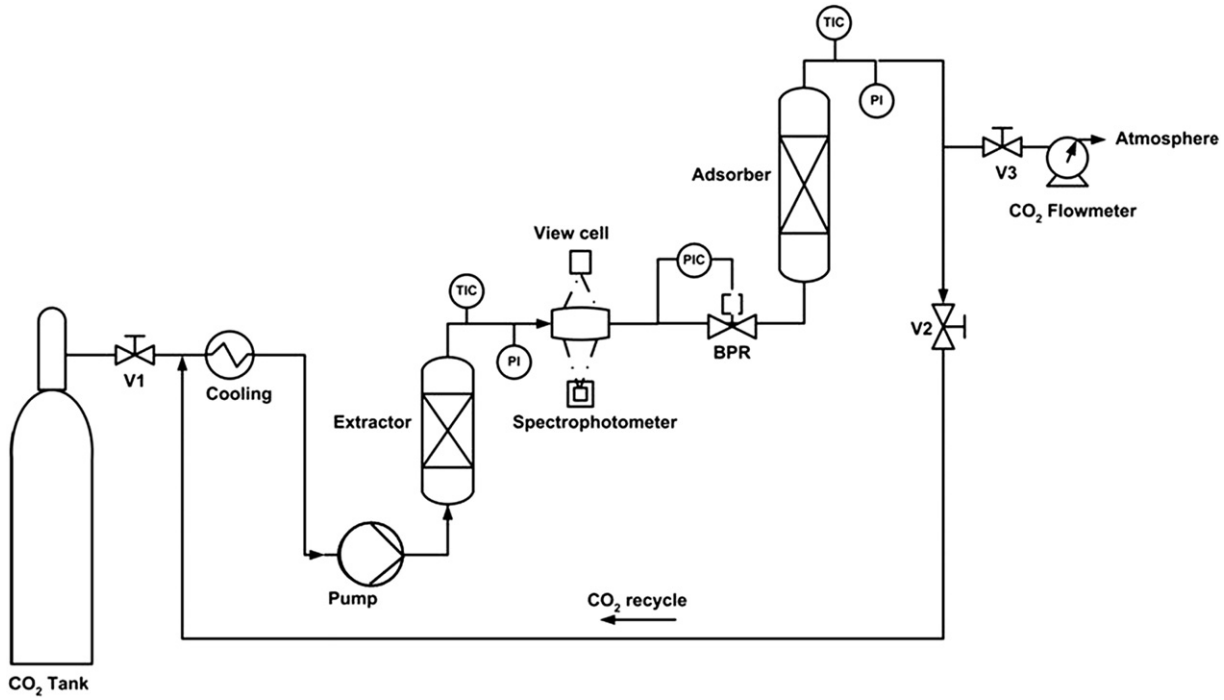

Fig. 1. Setup for a developed process that integrates extraction, impregnation and foaming steps.

material from which a target substance is to be extracted. The adsorption column is filled with solid to be impregnated by the extract from the prior extraction step. Electric heating enables heating of the extractor and adsorption vessel up to temperatures of $T_{max} = 100$ °C. The CO_2 is pumped into the extractor until the required pressure is obtained by a double acting pneumatically driven piston pump. In case of supercritical extraction of the *Usnea* lichen, the conditions are set to 30 MPa and 40 °C. Additionally, a view cell ($T_{max} = 120$ °C, $P_{max} = 50$ MPa, window diameter 18 mm) is connected to the extractor outlet and equipped with a microspectrophotometer (Ocean Optics, model USB4000 Miniature Fiber Optic Spectrometer) for inline detection of changes in solute concentration. The temperature inside the adsorption vessel containing PCL is set to 35 °C. A manual back pressure valve TESCOM (BPR) is used for pressure regulation within the CO_2-cycle between the extractor and adsorption vessels. A CO_2 flow meter (Ritter, Germany) is provided to indicate the consumption of CO_2 passing through the system.

The procedure for every test is characterized by two variables of time, t_1 and t_2, where t_1 is the time of continuous extraction–adsorption in a single passing mode at given conditions (Extraction: 30 MPa/40 °C and Adsorption:17 MPa/35 °C or 30 MPa/40 °C) and t_2 represents the time of recycling of the solution at the adsorption conditions through both extractor and adsorption vessel. The impregnation percentage was calculated using Eq. (2).

$$I(\%) = \frac{m_e}{m_e + m_c} \cdot 100 \quad (2)$$

Where m_e is the lichen extract mass incorporated into the sample and determined by a gravimetric procedure. It represents the mass change of the composite before and after processing. Initial mass of the composite is denoted as m_c.

2.5. Characterization techniques

Apart from the High Pressure Differential Scanning Calorimetry (HP-DSC) described above, DSC measurements were performed at atmospheric pressure on samples after $scCO_2$ processing with a Shimadzu DSC-50 thermal analyzer under nitrogen atmosphere at a heating rate of 10 °C/min, from room temperature to 120 °C. From DSC curves the crystallinity of PCL phase in the foamed composite (X_c) was determined using a heat of fusion value (ΔH_{100}) of 135.31 J/g [35] for 100% crystalline PCL according to Eq. (1).

Thermogravimetric analysis was carried out with a thermobalance model TGA 50 (Shimadzu) in the temperature range of 25–1000 °C, using alumina crucibles, under dynamic air atmosphere (30 mL min^{-1}) and heating rate of 10 °C·min^{-1}. HA content wt/wt.% in the composites was determined from the obtained curves.

Density values of the PCL and PCL–HA scaffolds were determined by using a Sartorius Balance (YDK01) with a density kit. The porosity (P) represents the "void space" of the scaffold and was calculated from the density of the scaffold δS = (scaffold weight/scaffold volume) and the theorical density of the composites ($\delta_{composite}$) considering $\delta_{PCL} = 1.14$ g/cm^3 and $\delta_{HA} = 3.16$ g/cm^3. (Eq. (3)).

$$P = \left(1 - \frac{\delta S}{\delta \text{composite}}\right) \times 100 \quad (3)$$

Raman microspectrometric analyses of composites were performed on a multichannel Renishaw In Via Reflex microspectrometer. Excitation was provided by the 514 nm line of an Ar laser. To achieve an enhanced signal-to-noise ratio, 30–50 scans were accumulated, each of 15 s exposure time with laser power ranging between 30 and 300 mW.

Morphology of the samples was investigated by scanning electron microscopy (SEM), employing a Jeol JXA-8600 microscope after coating the samples with a thin gold layer. The obtained images were analyzed by means of the access imaging software tool, ImageJ, in order to describe morphology and pore diameter of the obtained materials.

2.6. Determination of the antibacterial activity of impregnated PCL scaffolds

The modified broth macrodilution method was used for the investigation of antibacterial activity of impregnated PCL–HA composites and Cation Adjusted Mueller Hinton Broth (CAMHB, Becton Dickinson) was used as a standard culture medium. The assays were performed in sterile 13 × 100 mm glass tubes, by using PCL–HA concentrations of 100–200 mg/mL. The assay was performed by triplicate, during

incubation time of 24 h, at 37 °C. A standardized inoculum of investigated strain (MRSA ATCC 43300) was prepared by suspending colonies directly in CAMHB to the same density as 0.5 McFarland turbidity standard (approximately 1–3.10^8 Colony-forming Units/mL [CFU/mL]). Serial 1:10 dilutions of this suspension were made and inoculum sizes of 3–4.10^4 CFU/mL and 2 × 10^5 CFU/mL were used as initial CFU numbers in these tests. Controls without PCL–HA and with non-impregnated PCL were also analyzed. The total number of bacteria after incubation (CFU/mL) was determined by plate counts for each microorganism. The mean value for Log (CFU/mL) was registered for each sample ($P < 0.05$).

3. Results and discussion

3.1. Behavior of PCL and PCL–HA composites under CO_2 pressure

In presence of compressed carbon dioxide it is well known that the melting temperature, Tm, of a semicrystalline polymer is usually depressed with respect to its value at atmospheric pressure [19,36]. Fig. 2 shows the effect of pressure on the melting temperature and crystallinity of pure PCL. As expected, the melting temperature is decreased by CO_2 entering the polymer matrix up to a saturation pressure from where there is no significant influence of the pressure. An almost abrupt transition from a linear behavior of Tm on pressure to a nearly constant value becomes apparent. The slope of the linear section depends on the compressibility of the condensed phases, as well as of the diluent [36]. The "kink" point which refers to the change in the slope and commonly represents the lowest value of the depressed melting point for the neat PCL was at pressure of 10 MPa (Fig. 2a). The obtained values coincide with literature although due to the optical method used Tm-values of Lian et al. [36] are slightly higher since only the fully melted state is detected by the light transmission method they applied.

Similar results have been reported by Reigner et al. [37] who applied HP-DSC at pressures only up to 4.83 MPa. The melting behavior at moderate and high pressure arises from the opposed effects of the solubility which leads to the decreasing melting temperature on the one hand and the hydrostatic pressure which causes Tm to increase on the other [38]. Reportedly, CO_2 rapidly dissolves into polymers at moderate pressures (8–10 MPa), and the solubility of CO_2 linearly increases with pressure [38,39]. The solubility effect is dominant in the moderate pressure range while the hydrostatic pressure effect becomes significant at higher pressures when the polymer becomes saturated and the solubility of CO_2 reaches a constant value [39]. After the transition at 10 MPa a slightly increasing Tm was observed up to 17 MPa (Fig. 2a). This behavior has been explained by several phenomena: lamellar thickening due to the enhancement of the chain mobility upon dissolution of CO_2 in the polymer [36], changes in the magnitude of the hydrostatic pressure effect [40] and the possible extraction of the low molecular weight fractions [38].

Another advantage of the used HP-DSC method is the possibility of determining the change in crystallinity in situ. The effect of the pressure on crystallinity of PCL determined by HP-DSC in the range of 0.1–17 MPa is shown in Fig. 2b. A linearly decreasing crystallinity ($d\chi_c/dp = -5.93\%$ / MPa) was observed within the pressure range of 0.1–5.5 MPa. At 5.5 MPa a transition is observed beyond which crystallinity increases. Mechanisms that govern crystallization and the melting processes are both related to the chain mobility of the amorphous phase which surrounds the crystallites.

As a consequence it is expected that the crystallization temperature decreases linearly with increasing CO_2 pressure as long as the compaction effect caused by the hydrostatic pressure remains small enough [37].

The prepared PCL–HA composites by solvent casting were also analyzed by HP-DSC for interpreting the diffusion of CO_2 into the sample. DSC curves determined at 17 MPa are shown in Fig. 3 for the 10 wt.% HA-composites and a DSC curve for pure PCL are included for comparison. The composites PCL–HA(N) and PCL–HA(M) show a melting temperature slightly lower than the pure PCL, while the PCL–HA(S) shows a Tm even lower than these (Table 1). These values reflect that the Tm cannot be directly associated with the degree of crystallinity at the processing conditions but rather with the filler-matrix interaction [31]. Apparently an increase in solubility of CO_2 into PCL–HA(S) is expected,

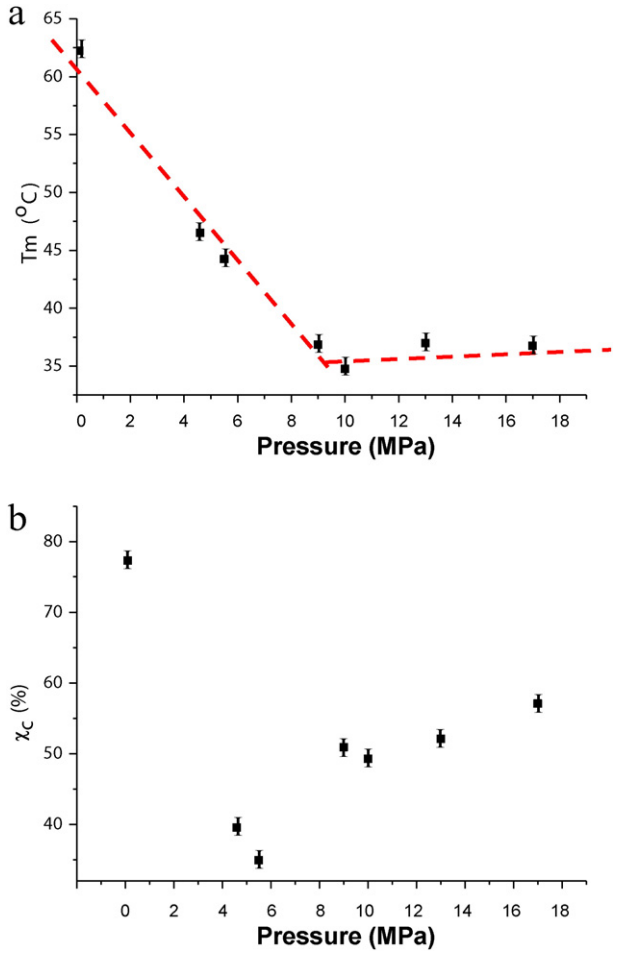

Fig. 2. (a) Depression in the melting temperature of PCL as a function of CO_2 pressure determined by HP-DSC data. (b) Crystallinity [χ_c] of pure PCL at different pressures of CO_2.

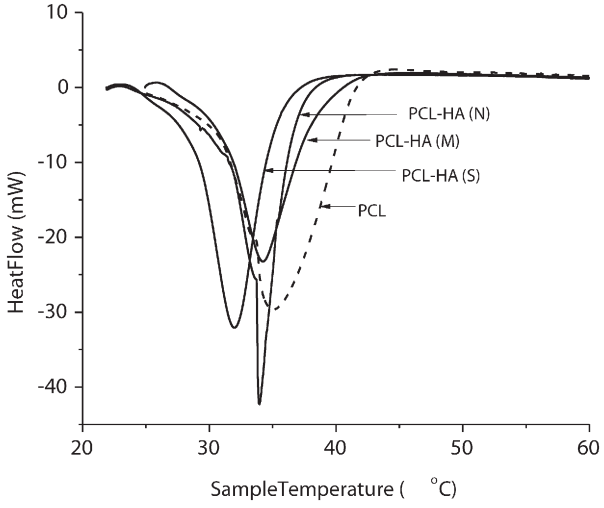

Fig. 3. HP-DSC curves for PCL–HA10 wt.% (particle size influence) at 17 MPa. (N: 1 μm); (S:5 μm); (M:10 μm).

Table 1
Influence of HA powder (N, M, S) (10–20%) on Tm depression, ΔHm and χ_c of PCL–HA in presence of $scCO_2$ at 17 MPa.

Sample	HA (%)[a]	Tm [°C]	ΔHm [J/g]	χ_c [%]	Onset T [°C]	Offset T [°C]
PCL	0	36.75	53.57	39.59	32.94	41.43
PCL + HA(N)	10	35.58	42.90	31.70	33.60	35.87
PCL + HA(S)	10	35.13	39.40	29.12	30.44	36.33
PCL + HA(M)	10	35.87	41.51	30.68	30.76	38.51
PCL + HA(M)	20	35.62	35.38	26.15	32.03	39.07

[a] Nominal content of HA powder respect to the composite mass.

probably due to filler particle agglomeration on a scale of few micrometers (not observed by SEM). The effect of adding HA particles into the PCL matrix on the degree of crystallinity of PCL is quantified in Table 1. The presence of HA filler within the PCL matrix obviously decreases crystallinity, which is further reduced as the content increases. Among different particle sizes and procedures there is no significant effect except for the nano particles, the peak of melting in DSC curves is the most narrow one reflecting a homogeneous crystalline structure. As a summary it can say that the crystallinity of PCL–HA decreased in the following order: PCL–HA(N) > PCL–HA(M) > PCL–HA(S) (Table 1). Also, crystallinity showed tendency to decrease as the HA amount increases: PCL > PCL–HA(M10) > PCL–HA(M20) (Table 1). This study shows that a good interaction between PCL matrix and HA particles with micrometric size can be achieved by a simple preparation method such as solvent casting. The difficulty of obtaining homogeneous composites with a very high percentage of HA(N) particles by solvent casting, and the good interaction between the PCL matrix and HA(M) particles observed by DSC analysis suggests to use the PCL–HA(M) composites for the following functionalization process. PCL–HA(M) samples with 10 wt/wt.% and 20 wt/wt.% HA were chosen for further processing to obtain the antibacterial scaffolds.

3.2. Impregnation and foaming of PCL–HA(M) composites by integrated supercritical process

Table 2 shows the processing conditions according to the process described above, the nominal and measured wt% of HA, the wt% of impregnation (I %) and the density of the obtained PCL–HA(M) foams. For comparison, $scCO_2$ treated PCL samples without impregnation are also presented. Variations in P and T of the integrated process appear to affect the final density of the composites. At higher pressure and temperature, a decreasing density of the composites was observed. At these processing conditions, viscosity of the composite system is reduced which favors the nucleation and growth of bubbles during depressurization. The density of the scaffolds can be varied by adapting the CO_2 pressure and temperature as well as the filler content.

Table 2
Experimental conditions for integrated process (P, T, t_1 and t_2), wt.% of HA (nominal and TGA determined), density and wt.% impregnation (wt% I) on PCL and PCL–HA foams.

Sample	wt.% HA[a]	wt.% HA[b]	$P_{adsorption}$ [MPa]	$T_{adsorption}$ [°C]	Procedure	δ [g/cm^3]	wt.% I
M0-17/35	0	0	17	35	[23]	0.38	0
M0-17/35	0	0	17	35	t_1: 2 h t_2: 1 h	0.59	2.8
M10-17/35	10	11	17	35	t_1: 2 h t_2: 1 h	0.38	4.1
M10-30/40	10	8	30	40	t_1: 2 h t_2: 0 h	0.28	5.7
M20-17/35	20	15	17	35	t_1: 2 h t_2: 1 h	0.58	5.9
M20-30/40	20	12	30	40	t_1: 2 h t_2: 0 h	0.39	1.7

[a] Nominal content of HA used in the composite preparation.
[b] HA content determined by TGA in the composite before $scCO_2$ processing.

Table 2 lists the wt% of HA within the prepared composites determined by TGA analysis. In Fig. 4, the results of the TGA of a 20 wt.% HA sample are presented from which the actual content in HA is determined. Pure PCL presents a simple decomposition profile with a single transition temperature (i.e., 370–450 °C) (no shown). For the composites, PCL degrades within the characteristic temperature range observed for the pure polymer [41]. The HA content for each composite was determined from the residual mass after calcination at 1000 °C. Some differences were found between samples with the same nominal content of HA. This was associated to the preparation method, where evidently no good retention of the filler amount into the matrix is achieved, especially at higher HA contents. The measured density values are in accordance with the content of HA determined by TGA analysis, as an increased amount of HA enhances the density of the composite.

In Fig. 5 the porosity [*P* %, (Eq. (3))] is presented for each sample including the wt% of impregnation and of HA. It can be observed that increasing pressure and temperature favor a higher final porosity. However, the presence of a high content in HA particles obviously is decisive for generation of a high porosity after decompression. The sample that contains the maximum amount of HA (15 wt.% HA) reaches the lowest porosity value, however this porosity is still in a useful range as scaffold (approx. 60% of porosity).

The wt.% of impregnation was positively affected by increased porosity in the case of the composite with the lower nominal HA content (10%). On the contrary, the efficiency of impregnation decreased with increasing porosity in case of the composite containing a higher nominal amount of the HA (20%).

There seems to be an optimum in HA content that triggers additional sorption of the previously extracted components and which is not clearly related to the parameters of the impregnation process. In any case, the wt% of impregnation for the studied composites resulted in higher values than the impregnated amount of extract for PCL materials [26] by using the same process at comparable conditions of T y P. This higher efficiency using composite materials can be associated to the interface created between the filler and the polymeric matrix that allows improved sorption of the solution of CO_2 + extract.

The extraction and impregnation procedure including the simultaneous extraction (30 MPa/40 °C) and adsorption (17 MPa/35 °C) over 2 h followed by 1 h of homogenizing and flushing the solution throughout both, extractor and adsorber (rinsing) was applied, since this combination of operating conditions enabled the highest impregnation value of *Usnea* extract already in pure PCL [30]. In order to optimize the process regarding wt.% of impregnation and processing time, the pressure and temperature within the sorption column were increased and flushing was excluded. The increasing pressure and temperature inside the adsorber had a positive effect on the impregnation when PCL–HA with 10% of HA was applied. On the contrary, in case of the PCL–HA

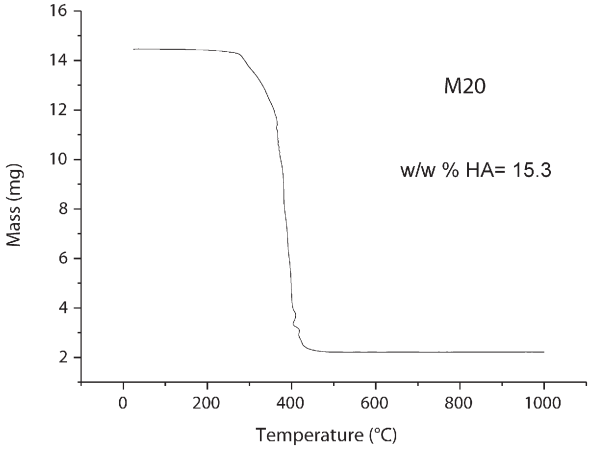

Fig. 4. TGA curves of M20 sample (PCL + 20 wt.% HA) without $scCO_2$ processing.

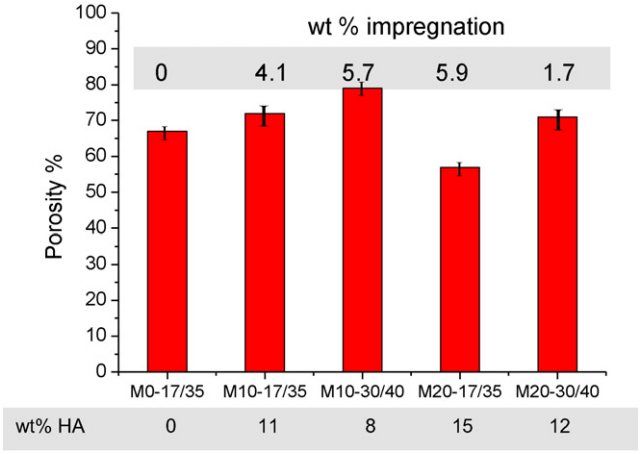

Fig. 5. Porosity of the obtained composite foams including the wt.% of impregnation and of HA.

with a higher amount of HA (20%), an increasing pressure and temperature in the sorption column resulted in a significant decreasing wt% of impregnation (Table 2). This might be due to a more inhomogeneous filler distribution.

Fig. 6 shows the microstructure of $scCO_2$ treated samples and virgin composites observed by SEM analyses. In all processed samples, an interconnected porous structure was observed. The samples processed at 35 °C and 17 MPa showed microstructures with a homogeneous distribution of macro and micropores (bi-modal distribution of pore size), which is desirable for a scaffold. The samples M10-30/40 showed no significant macroporosity, although showing a higher value of porosity.

As depicted in Fig. 7 the bands at 963 cm^{-1} (ν_1 PO_4), and weak signals at 609–592–581 cm^{-1} (ν_4 PO_4), 487–446–431 cm^{-1} (ν_2 PO_4) are characteristic to the HA [42]. The bands at 1724 cm^{-1} (ν C = O), 1470–1441–1419 cm^{-1} (δCH_2), 1305–1285 cm^{-1} (ωCH_2), 1110 cm^{-1} (skeletal stretching) and 912 cm^{-1} (ν C–COO) result uniquely from PCL. Both components, PCL as well as HA, contribute to the bands at 1065 and 1042 cm^{-1} (ν_3 PO_4 and PCL skeletal stretching). The Raman spectrum of pure PCL shows a higher intensity at 1419 and 1285 cm^{-1}, compared to the composites which is attributed to crystalline PCL. The ratio of the intensity between the bands at 1305 and 1285 cm^{-1} was identified as marker of crystallinity [13]. The ratios of the intensity between the bands prevalently due to HA and PCL (in particular I963/I1724) increase with respect to the amount of HA in the composite as expected. Differences in the measured intensities of the various spectra obtained from the porous samples are attributed to factors related with the assay (as the intensity variation, or the positioning of the sample). The trend of the spectra indicates that the polymer in the

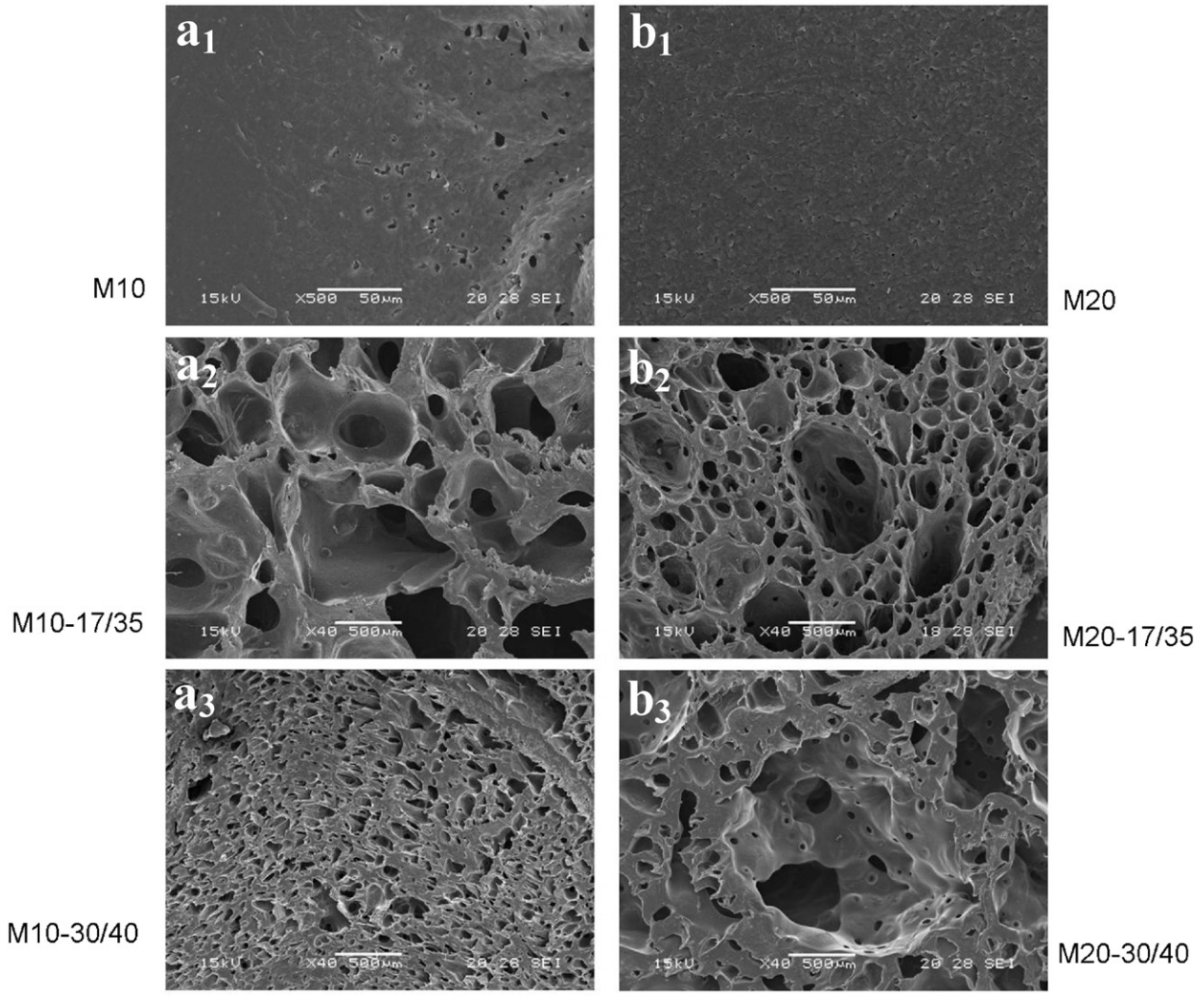

Fig. 6. Microstructures of the composites of PCL with 10 wt.% of nominal HA (a_1: no foamed; a_2: processed at 17 MPa and 35 °C; a_3: processed at 30 MPa bar and 45 °C) and 20 wt.% of nominal HA (b_1: no foamed; b_2: processed at 17 MPa and 35 °C; b_3: processed at 30 MPa and 45 °C).

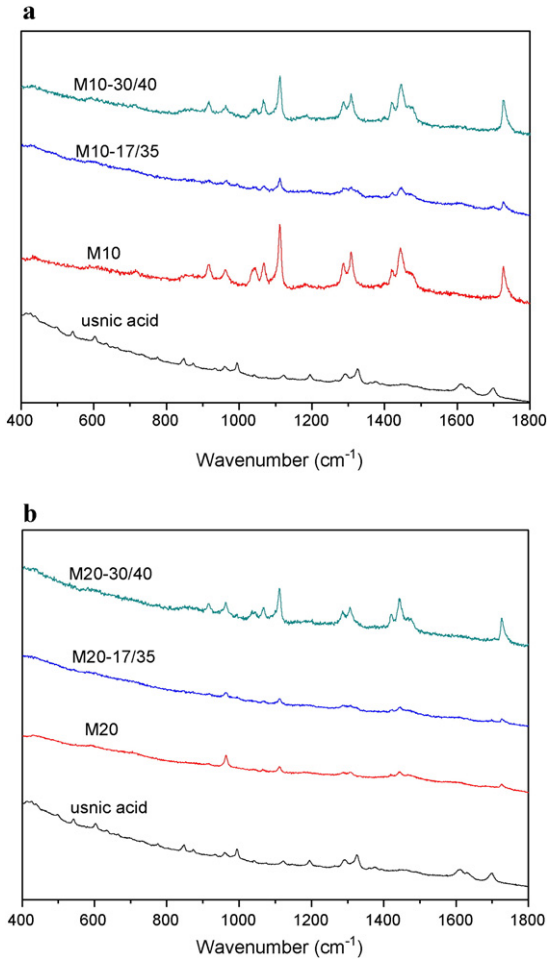

Fig. 7. Raman spectra of obtained composite foams of (a) PCL with 10 wt.% HA and (b) PCL with 20 wt.% HA.

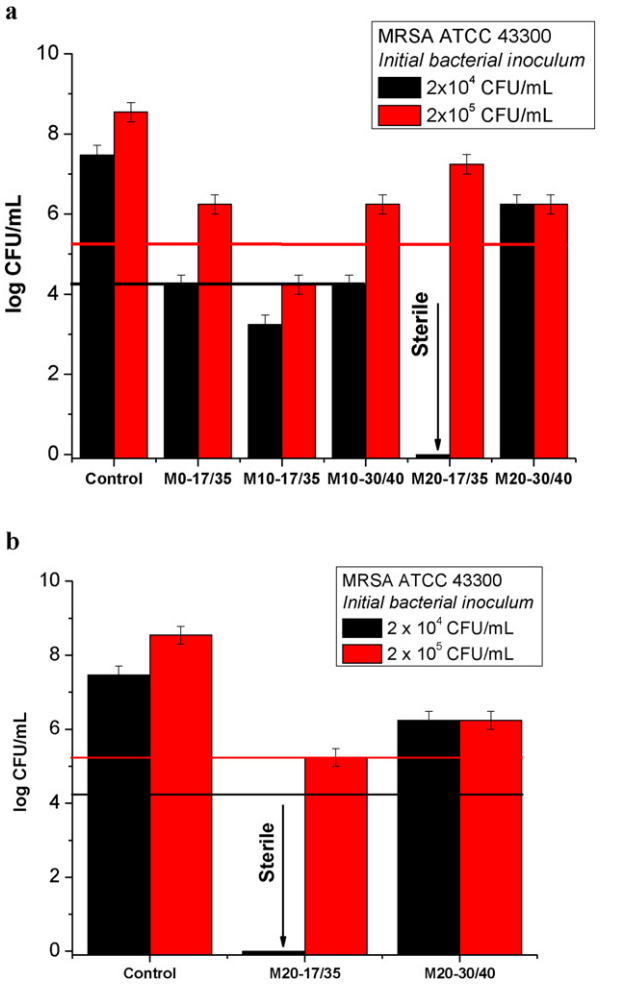

Fig. 8. Growth inhibition for MRSA by functionalized PCL–HA scaffolds with inoculated sample concentration of (a) 100 mg/mL and (b) 200 mg/mL (vertical bars represent means of three replicates with standard deviation. Control: culture medium without sample).

composite is more amorphous than the PCL starting material, in agreement with the DSC data (Table 2).

The Raman spectrum of usnic acid is presented in Fig. 7. The four main vibrational signals are situated in the area between 1700–1200 cm^{-1}. The band of 1694 cm^{-1} corresponds to $\nu C=O$ conjugated cyclic ketone group, the band at 1607 cm^{-1} is due to quadrant ring stretch, the strong band at 1322 cm^{-1} is assigned to the ring stretch, and the band at 1289 cm^{-1} is attributed to the antisymmetric ν(COC) aryl alkyl ether mode. Regarding the composition, Raman spectra did not reveal significant presence of the usnic acid in the processed composites. This means that the content of usnic acid probably is located within the polymer matrix or within the interface between the polymer and the inorganic filler but is not detected on the surface of the sample.

The efficiency of the functionalization of the PCL–HA scaffolds was further corroborated with testing antibacterial properties of obtained porous samples. The results of the antibacterial screening of the tested composites are presented in Fig. 8. In this investigation numbers of 10,000 CFU and 100,000 CFU were chosen as indubitable infectious dose of MRSA strains no matter whether other factors are present or not. The infectious dose is the amount of pathogenic organisms that will cause an infection in susceptible hosts. An antibacterial agent is defined as bactericidal when it exhibits the distinctive endpoint of causing a 99% reduction in bacterial inoculum within the 24-h period of exposure. Otherwise, it is considered bacteriostatic. The impregnated PCL–HA scaffolds exhibited a higher antibacterial activity when a low bacterial inoculum level (2×10^4 CFU/mL) was assayed except the M20-30/40 composite. According to Fig. 8a, the minimum wt.% of impregnation of 4.1% was needed for a bacteriostatic effect for the lower bacterial inoculum level. Only M10-17/35 showed a bacteriostatic effect at both bacterial inoculum levels (Fig. 8a). The M20-30/40 with the lowest wt.% of impregnation (1.7%) allowed development of the strain, although the growth was reduced by more than one logarithmic order with respect to the control.

A bactericidal effect was evidenced only for the M20-17/35 composite at both used inoculated sample concentrations (100 mg/mL and 200 mg/mL) (Fig. 8a and b, respectively). This was expected considering that M20-17/35 had the higher wt.% of impregnation of the *Usnea* extract (5.7 wt.%), and the higher filler retention (15 wt.% of HA) in comparison to the M20-30/40 (wt.% of impregnation of 1.7% and retained 12 wt.% of HA). Additionally, this composite showed the microstructure characterized by a bi-modal distribution of pore size (Fig. 6).

According to all the presented results, the following procedure for fabrication of the microporous PCL–HA scaffolds with high wt.% of *Usnea* extract impregnation and bacteriostatic and/or bactericidal effects against MRSA can be defined as suitable:

(a) Preparation of PCL–HA with 20 wt.% of nominal content of HA powder using solvent casting technique for production of 15 wt.% retained HA in the composite. Proper porosity (approx. 60%) is achieved after exposure to $scCO_2$ at 17 MPa and 35 °C.
(b) Processing conditions: 2 h of extraction (Extractor: 30 MPa/40 °C; Adsorber: 17 MPa/35 °C) followed by 1 h of rinsing at

17 MPa (both vessels) and depressurization rate at 0.5 MPa/min. These conditions enabled satisfactory high level of the *U. lethariiformis* extract incorporation (5.9%) and antibacterial effect is attained. The applied depressurization rate provided a bimodal distribution of pore size with homogeneous distribution of the extract in the scaffold.

4. Conclusions

Novel data on in situ melting temperature depression and crystallinity of PCL and PLC–HA under elevated pressures (4.6–17 MPa) were provided by using the high pressure DSC. The PCL–HA composites with nano- and micrometric HA particles (10 wt.%) had a somewhat lower melting range as well as crystallinity in comparison to pure PCL indicating a homogeneous distribution and good contact of HA inside the PCL matrix. The PCL–HA composites with micrometric HA particles were the most appropriate for the designated supercritical extraction and impregnation process due to the simplicity of preparation and other satisfactory properties. Especially the scaffold obtained from the PCL–HA with 20 wt.% of HA was shown to be promising regarding the quantity of impregnated active substance at 17 MPa and 35 °C (5.9%) and bactericidal effect on the tested MRSA strains. Also, the composites with 10 wt.% of HA might be of interest, as well due to a sufficient level of impregnation (4.1–5.7 wt.%) and bacteriostatic effect on the selected MRSA strains. Thus, the integrated extraction–impregnation process has been validated as suitable for functionalizing PCL–HA scaffolds with *Usnea* extract (up to 5.9 wt.%).

The future research will be focused on studying the $scCO_2$ solubility into PCL based carriers and relevant mass transfer phenomena in order to optimize this integrated extraction and impregnation process for incorporation of other natural bioactive agents.

Acknowledgments

The authors thank the following institutions for providing financial support: National Research Council (CONICET, Argentina) (Project PIP1851), University of Mar del Plata (Argentina) (Project 15G/388), Technical University of Hamburg, Hamburg (Germany) and Ministry of Education, Science and Technological Development of the Republic of Serbia (Project III45017).

References

[1] A.R. Amini, C.T. Laurencin, S.P. Nukavarapu, Bone tissue engineering: recent advances and challenges, Crit. Rev. Biomed. Eng. 40 (2013) 363–408.
[2] Y. Liu, J. Lim, S.H. Teoh, Review: development of clinically relevant scaffolds for vascularised bone tissue engineering, Biotechnol. Adv. 31 (2013) 688–705.
[3] A. Rezaei, M.R. Mohammadi, In vitro study of hydroxyapatite/polycaprolactone (HA/PCL) nanocomposite synthesized by an in situ sol–gel process, Mater. Sci. Eng. C 33 (1) (2013) 390–396.
[4] S. Eosoly, N.E. Vrana, S. Lohfeld, M. Hindie, L. Looney, Interaction of cell culture with composition effects on the mechanical properties of polycaprolactone–hydroxyapatite scaffolds fabricated via selective laser sintering (SLS), Mater. Sci. Eng. C 32 (8) (2012) 2250–2257.
[5] B. Chuenjitkuntaworn, W. Inrung, D. Damrongsri, K. Mekaapiruk, P. Supaphol, P. Pavasant, Polycaprolactone/hydroxyapatite composite scaffolds: preparation, characterization, and in vitro and in vivo biological responses of human primary bone cells, J. Biomed. Mater. Res. A 94 (2010) 241–251.
[6] L. Ji, W. Wang, D. Jin, S. Zhou, X. Song, In vitro bioactivity and mechanical properties of bioactive glass nanoparticles/polycaprolactone composites, Mater. Sci. Eng. C 46 (2015) 1–9.
[7] Hydroxyapatite and Related Materials, CRC Press, Inc., Boca Raton, FL, USA, 1994 (ISBN 0-8493r-r4750-5).
[8] C. Vallo, P.E. Montemartini, M.A. Fanovich, J.M. Porto López, T.R. Cuadrado, Polymethylmethacrylate-based bone cement modified with hydroxyapatite, J. Biomed. Mater. Res. B Appl. Biomater. 48 (1999) 150–158.
[9] F. Liu, R. Wang, Y. Cheng, X. Jiang, Q. Zhang, M. Zhu, Polymer grafted hydroxyapatite whisker as a filler for dental composite resin with enhanced physical and mechanical properties, Mater. Sci. Eng. C 33 (8) (2013) 4994–5000.
[10] M.A. Woodruff, D.W. Hutmacher, The return of a forgotten polymer—polycaprolactone in the 21st century, Prog. Polym. Sci. 35 (2010) 1217–1256.
[11] L. Shor, S. Güçeri, X. Wen, M. Gandhi, W. Sun, Fabrication of three-dimensional polycaprolactone/hydroxyapatite tissue scaffolds and osteoblast-scaffold interactions in vitro, Biomaterials 28 (2007) 5291–5297.
[12] X. Xiao, R. Liu, Q. Huang, X. Ding, Preparation and characterization of hydroxyapatite/polycaprolactone-chitosan composites, J. Mater. Sci. Mater. Med. 20 (2009) 2375–2383.
[13] P. Taddei, A. Tinti, M. Reggiani, C. Fagnano, In vitro mineralization of bioresorbable poly(ε-caprolactone)/apatite composites for bone tissue engineering: a vibrational and thermal investigation, J. Mol. Struct. 744–747 (2005) 135–143.
[14] D. Choi, K.G. Marra, P.N. Kumta, Chemical synthesis of hydroxyapatite/poly(ε-caprolactone) composites, Mater. Res. Bull. 39 (2004) 417–432.
[15] Y. Wang, L. Liu, S. Guo, Characterization of biodegradable and cytocompatible nano-hydroxyapatite/polycaprolactone porous scaffolds in degradation in vitro, Polym. Degrad. Stab. 95 (2010) 207–213.
[16] E. Reverchon, S. Cardea, Supercritical fluids in 3-D tissue engineering, J. Supercrit. Fluids 69 (2012) 97–107.
[17] E. Reverchon, S. Cardea, Production of controlled polymeric foams by supercritical CO_2, J. Supercrit. Fluids 40 (2007) 144–152.
[18] M. Karimi, M. Heuchel, T. Weigel, M. Schossig, D. Hofmann, A. Lendlein, Formation and size distribution of pores in poly(ε-caprolactone) foams prepared by pressure quenching using supercritical CO_2, J. Supercrit. Fluids 61 (2012) 175–190.
[19] E. Kiran, K. Liu, K. Ramsdell, Morphological changes in poly(ε-caprolactone) in dense carbon dioxide, Polymer 49 (2008) 1853–1859.
[20] E. Marsich, F. Bellomo, G. Turco, A. Travan, I. Donati, S. Paoletti, Nano-composite scaffolds for bone tissue engineering containing silver nanoparticles: preparation, characterization and biological properties, J. Mater. Sci. Mater. Med. 24 (2013) 1799–1807.
[21] V. Mouriño, J.P. Cattalini, A.R. Boccaccini, V. Mourin, Metallic ions as therapeutic agents in tissue engineering scaffolds: an overview of their biological applications and strategies for new developments, J. R. Soc. Interface 9 (68) (2012) 401–419.
[22] S. Milovanovic, M. Stamenic, D. Markovic, M. Radetic, I. Zizovic, Solubility of thymol in supercritical carbon dioxide and its impregnation on cotton gauze, J. Supercrit. Fluids 84 (2013) 173–181.
[23] M.A.A. Meireles, Extraction of bioactive compounds from Latin American plants, in: José L. Martínez (Ed.), Chapter 8 in Supercritical Fluid Extraction of Nutraceuticals and Bioactive Compounds, CRC Press, Taylor & Francis Group, Boca Raton, FL-USA, ISBN: 0-8493-7089-2 2008, pp. 243–274.
[24] I. Zizovic, J. Ivanovic, D. Misic, M. Stamenic, S. Djordjevic, J. Kukic-Markovic, S.D. Petrovic, SFE as a superior technique for isolation of extracts with strong Antibacterial activities from lichen *Usnea barbata* L. J. Supercrit. Fluids 72 (2012) 7–14.
[25] M.M.R. de Melo, A.J.D. Silvestre, C.M. Silva, Supercritical fluid extraction of vegetable matrices: applications, trends and future perspectives of a convincing green technology, J. Supercrit. Fluids 92 (2014) 115–176.
[26] M.A. Fanovich, J. Ivanovic, P.T. Jaeger, An integrated supercritical extraction and impregnation process for production of antibacterial scaffolds, in: C. Domingo, P. Subra (Eds.), Supercritical Fluid Nanotechnology: Advances and Applications in Composites and Hybrid Nanomaterials, Pan Stanford Publishing Pte Ltd., 2015 (in press).
[27] E. Markočič, M. Škerget, Ž. Knez, Solubility and diffusivity of CO2 in poly(L-lactide)–hydroxyapatite and poly(D, L-lactide-co-glycolide)–hydroxyapatite composite biomaterials, J. Supercrit. Fluids 55 (2011) 1046–1051.
[28] J. Crank, G.S. Park, Methods of measurement, in: J. Crank, G.S. Park (Eds.), Diffusion in Polymers, Academic Press, New York 1968, pp. 1–39.
[29] A. Salerno, E. Di Maio, S. Iannace, P.A. Netti, Solid-state supercritical CO_2 foaming of PCL and PCL–HA nano-composite: effect of composition, thermal history and foaming process on foam pore structure, J. Supercrit. Fluids 58 (2011) 158–167.
[30] M.A. Fanovich, J. Ivanovic, D. Misic, M.V. Alvarez, P. Jaeger, I. Zizovic, Development of polycaprolactone scaffold with antibacterial activity by an integrated supercritical extraction and impregnation process, J. Supercrit. Fluids 78 (2013) 42–53.
[31] A. Salerno, S. Zeppetelli, E. Di Maio, S. Iannace, P.A. Netti, Novel 3D porous multiphase composite scaffolds based on PCL, thermoplastic zein and ha prepared via supercritical CO2 foaming for bone regeneration, Compos. Sci. Technol. 70 (2010) 1838–1846.
[32] M.A. Fanovich, P. Jaeger, Sorption and diffusion of compressed carbon dioxide in polycaprolactone for the development of porous scaffolds, Mater. Sci. Eng. C 32 (2012) 961–968.
[33] M.A. Giardina, M.A. Fanovich, Synthesis of nanocrystalline hydroxyapatite from $Ca(OH)_2$ and H_3PO_4 assisted by ultrasonic irradiation, Ceram. Int. 36 (2010) 1961–1969.
[34] A. López-Macipe, J. Gómez-Morales, R. Rodríguez-Clemente, Nanosized hydroxyapatite precipitation from homogeneous calcium/citrate/phosphate solutions using microwave and conventional heating, Adv. Mater. 10 (1998) 49–53.
[35] S. Jiang, X. Ji, L. An, B. Jiang, Crystallization behavior of PCL in hybrid con ® ned environment, Polymer 42 (2001) 3901–3907.
[36] Z. Lian, S.A. Epstein, C.W. Blenk, A.D. Shine, Carbon dioxide-induced melting point depression of biodegradable semicrystalline polymers, J. Supercrit. Fluids 39 (2006) 107–117.
[37] J. Reignier, R. Gendron, M.F. Champagne, Autoclave foaming of poly(—caprolactone) using carbon dioxide: impact of crystallization on cell structure, J. Cell. Plast. 43 (2007) 459–489.
[38] E. De Paz, S. Rodrı, J. Herreras, Determination of phase equilibrium (solid–liquid–gas) in poly-(ε-caprolactone)-carbon dioxide systems, J. Chem. Eng. Data 55 (2010) 2781–2785.
[39] S. Takahashi, J.C. Hassler, E. Kiran, Melting behavior of biodegradable polyesters in carbon dioxide at high pressures, J. Supercrit. Fluids 72 (2012) 278–287.
[40] E. Weidner, V. Wiesmet, M. Skerget, Phase equilibrium (solid–liquid–gas) in polyethyleneglycol–carbon dioxide systems, J. Supercrit. Fluids 10 (1997) 139–147.

[41] A. Mohamed, S.H. Gordon, G. Biresaw, Polycaprolactone/polystyrene bioblends characterized by thermogravimetry, modulated differential scanning calorimetry and infrared photoacoustic spectroscopy, Polym. Degrad. Stab. 92 (7) (2007) 1177–1185.

[42] C.G. Kontoyannis, N.C. Bouropoulos, P.G. Koutsoukos, Raman spectroscopy: a tool for the quantitative analysis of mineral components of solid mixtures. The case of calcium oxalate monohydrate and hydroxyapatite, Vib. Spectrosc. 15 (1997) 53–60.